New Day in Medicine
Новый День в Медицине

NDM

TIBBIYOTDA YANGI KUN

Ilmiy referativ, marifiy-ma'naviy jurnal

AVICENNA-MED.UZ

ISSN 2181-712X.
EiSSN 2181-2187

2 (88) 2026

ТИББИЁТДА ЯНГИ КУН
НОВЫЙ ДЕНЬ В МЕДИЦИНЕ
NEW DAY IN MEDICINE

Илмий-рефератив, маънавий-маърифий журнал
Научно-реферативный,
духовно-просветительский журнал

УЧРЕДИТЕЛИ:

БУХАРСКИЙ ГОСУДАРСТВЕННЫЙ
МЕДИЦИНСКИЙ ИНСТИТУТ
ООО «ТИББИЁТДА ЯНГИ КУН»

Национальный медицинский
исследовательский центр хирургии имени
А.В. Вишневского является генеральным
научно-практическим
консультантом редакции

Журнал был включен в список журнальных
изданий, рецензируемых Высшей
Аттестационной Комиссией
Республики Узбекистан
(Протокол № 201/03 от 30.12.2013 г.)

2 (88)

2026

февраль

www.bsmi.uz
https://newdaymedicine.com
E: ndmuz@mail.ru
Тел: +99890 8061882

Received: 20.01.2026, Accepted: 06.02.2026, Published: 10.02.2026

UDK 617.52-006

SPATIAL ACCURACY ANALYSIS OF VSP-GUIDED MANDIBULAR RECONSTRUCTION: A THREE DIMENTIONAL REGIONAL ANALYSIS OF SURGICAL DEVIATION IN COMPLEX DEFECTS

[1]Ismailov Mukhammad Rustamboy ugli https://orcid.org:0009-0004-6577-5680
e-mail: antiboof521@gmail.com
[2,3]Mustafaev Ummatjon Gayrat ugli https://orcid.org/0000-0002-1141-8467 *e-mail:* dr.ummatm@gmail.com
*[1]Maimaitituxun Tuerdi** https://orcid.org/0000-0002-0505-0993 *e-mail:* maimaitituxun@aliyun.com*
[4]Khatamov Erkin Beknazarovich https://orcid.org/0009-0002-9652-5524
*e-mail:*erkinkhatamovsam@gmail.com
[1]Aidos Rakhizayev https://orcid.org/0009-0004-2602-3478 *e-mail:* aidos2911@cloud.com

[1]Department of Oral and Maxillofacial Surgery First Affiliated Hospital of Xinjiang Medical University, Urumqi, Xinjiang, 830011, PR China,
[2] School of Pharmacy, Xinjiang Medical University, Urumqi, 830011, PR China,
[3] Department of Chemistry and Pharmacy, Alfraganus University, Tashkent, 100190, Uzbekistan
[4] Department of maxillofacial surgery and reconstructive plastic surgery, Samarkand State Medical University Multidisciplinary Clinic, Samarkand, Uzbekistan
Corresponding Authors: Maimaitituxun T. https://orcid.org/0000-0002-0505-0993
e-mail: maimaitituxun@aliyun.com*

✓ ***Resume***

***Objective:** To quantify the three-dimensional spatial accuracy of virtual surgical planning (VSP)-guided fibula free flap mandibular reconstruction and to characterize the directional distribution of residual geometric errors across anatomical zones through axis-specific decomposition, with particular focus on secondary and complex defects.*

***Materials and Methods:** A retrospective analysis was conducted on 12 consecutive patients (mean age 45.8 ± 14.8 years; range 17–78) who underwent segmental mandibular resection and vascularized fibula free flap reconstruction between February 2024 and December 2025. A standardized CAD/CAM workflow was employed, incorporating patient-specific SLA cutting guides and pre-operatively adapted 2.4 mm titanium reconstruction plates contoured against stereolithographic resin mandibular models. Postoperative CBCT datasets were registered against the preoperative virtual plan in Materialise 3-matic software, with superimposition anchored on unoperated native mandibular regions. Deviations were decomposed along the mediolateral (X), superoinferior (Y), and anteroposterior (Z) axes. Patients were stratified by the Brown classification into less complex (Class I–II, n=6) and complex (Class III–IV, n=6) subgroups, and between-group differences were evaluated by independent samples t-test.*

***Results:** The mean global 3D deviation across the cohort was 3.40 ± 1.02 mm. No statistically significant difference was identified between the less complex (3.55 ± 1.12 mm) and complex (3.29 ± 1.10 mm) subgroups (P > 0.05), confirming that defect severity does not adversely affect overall reconstructive accuracy when a standardized digital workflow is employed. Axis-specific analysis, however, revealed pronounced and anatomically localized failure patterns not captured by global metrics. Posterior proximal segments (condyle and ramus) accounted for 83% of maximum deviations, with errors manifesting as two mechanically distinct transverse displacement patterns: medial collapse in five patients, driven by unopposed medial pterygoid contractile forces, and lateral flaring in four patients following condylectomy, with a maximum lateral displacement of 9.13 mm in the neocondyle case (Patient 5, absolute maximum 12.10 mm). Inferior displacement of the anterior arch was identified in seven of twelve cases along the Y-axis, with a maximum vertical drop of 6.98 mm attributable to gravitational loading from the fascio-cutaneous paddle combined with suprahyoid muscular traction. Posterior symphyseal drift of 10.38 mm was recorded in one case following hardware destabilization and unopposed digastric contraction. Signed mean deviations along the X- and Y-axes approached zero due to cancellation of opposing directional errors, whereas absolute mean deviations reached 4.50 ± 2.91 mm*

(posterior ΔX) and 3.78 ± 1.51 mm (anterior ΔY), demonstrating that aggregate global scores systematically mask clinically significant zone-specific displacements.

Conclusion: The combined VSP, SLA cutting guide, and pre-bent plate protocol achieves reproducible global accuracy across a spectrum of defect complexities, including salvage reconstructions, at a cost-effective alternative to patient-specific milled implants. However, axis-specific analysis demonstrates that this protocol does not neutralize postoperative muscular forces on isolated bone segments. Biomechanical vulnerability is governed by anatomical location and local muscular force environment rather than overall defect size. Proximal segment instability — manifesting as medial collapse or lateral flaring — and anterior arch inferior displacement constitute distinct, targetable failure modes requiring adjunctive intraoperative fixation strategies, including temporary maxillomandibular fixation and condylar seating maneuvers, beyond standard cutting guide application.

Key words: Mandibular reconstruction; Virtual Surgical Planning (VSP); Fibula free flap; CAD/CAM; Stereolithography (SLA); Directional error analysis; Biomechanics; Condylar reconstruction; Brown classification; Medial collapse; Lateral flaring; Reconstruction plate; Osteotomy.

Relevance

Segmental mandibular reconstruction aims to restore skeletal continuity, masticatory function, and facial symmetry following oncological resection or osteonecrosis. The vascularized fibula free flap remains the current gold standard for this indication, providing reliable bicortical bone stock and a consistent vascular pedicle [1]. Its extensive application across a range of oncological and trauma settings has established it as the primary reconstructive modality for complex segmental mandibular defects [2,3]. Contouring a linear fibular graft to replicate the three-dimensional curvature of the native mandible presents a significant technical challenge; geometric inaccuracies in plate adaptation can result in condylar malpositioning, occlusal discrepancy, and facial asymmetry [4].

Virtual surgical planning (VSP) addresses the geometric complexity of fibula contouring by enabling digital pre-operative simulation of osteotomy configurations and plate adaptation. [5] CAD/CAM software platforms are now used across major reconstructive centres to generate patient-specific cutting guides that transfer the digital plan into the operating environment with measurable precision. [6] Comparative studies have confirmed that VSP-guided workflows reduce intraoperative time and improve morphological accuracy relative to conventional freehand contouring techniques [7,8].

Despite the demonstrated advantages of VSP, the translation of a digital plan into a physical reconstruction is subject to multiple sources of intraoperative error. Soft tissue tension and scar contracture exert unpredictable forces on bone segments [9]. Progressive scar formation within the operative field further compounds these forces through cicatricial contracture of the peri-osseous soft tissue envelope [10]. Achieving rigid stabilization of a short proximal ramus segment following condylectomy presents a recognized technical challenge due to the limited residual bone stock available for fixation and the absence of native articular constraint [11,12].

The existing literature on VSP accuracy predominantly reports global mean deviation metrics, without stratification by anatomical region or directional axis. This approach does not capture which specific zones are most susceptible to displacement, nor the directional nature of those errors. This gap in the literature is particularly relevant for complex defects involving the ramus and condyle, where biomechanical instability is greatest. A region-specific directional analysis is therefore required to identify the mechanistic basis of reconstructive failure and to guide the development of more effective intraoperative fixation strategies.

We designed this study to measure the true surgical fidelity of VSP-guided reconstructions.

We mapped 3D directional deviations along the X, Y, and Z axes. We compared preoperative digital plans with final postoperative CT scans. Heatmap and vector analyses helped pinpoint which anatomical zones are most vulnerable to shifting. Professor Mamatursin Turdi supervised every procedure at the First Affiliated Hospital of Xinjiang Medical University to maintain a standardized technique.

Materials and methods

2.1 Study Design and Ethical Considerations

This retrospective study was conducted at the First Affiliated Hospital of Xinjiang Medical University, Department of Oral and Maxillofacial Trauma and Orthognathic Surgery. Clinical records were reviewed for the period from February 2024 to December 2025. The study was approved by the institutional ethics committee and conducted in accordance with the Declaration of Helsinki. Written informed consent was obtained from all participants prior to surgical intervention.

2.2 Patient Selection

Eligible patients were those requiring segmental mandibular resection and reconstruction with a vascularized fibula free flap for benign or malignant pathology, osteonecrosis, or failed prior reconstruction. All cases required a complete VSP workflow implemented via CAD/CAM software. High-resolution pre- and postoperative CT imaging was mandatory for inclusion. Secondary and salvage cases, including those without preserved native anatomical landmarks, were deliberately included to represent the full clinical spectrum of reconstructive complexity. Cases with incomplete radiographic records were excluded. The final cohort comprised 12 consecutive patients.

2.3 Virtual Surgical Planning and Guide Fabrication

Pre-operative helical CT imaging (slice thickness ≤ 1.0 mm) was performed for all patients. The resulting DICOM datasets were imported into Materialise 3-matic software for segmentation and three-dimensional model reconstruction. The surgical team delineated resection margins, performed a virtual segmental mandibulectomy, and designed the fibular osteotomy configuration to replicate the patient's native mandibular contour. Patient-specific cutting and positioning guides were generated from the finalized virtual plan and fabricated in-house using an SLA 3D printer with biocompatible medical-grade resin. Standard 2.4 mm titanium reconstruction plates were pre-operatively adapted to stereolithographic resin models of the mandible, establishing a physical contouring template prior to surgical intervention.

2.4 Surgical Protocol

A simultaneous two-team approach was employed. The oncological team performed the segmental resection under guidance of the patient-specific cutting guides, after which the pre-bent reconstruction plate was secured to the remaining native mandible via pre-drilled index screw positions, establishing a fixed spatial reference frame. Concurrently, the reconstructive team harvested the fibula and executed the planned osteotomies using the corresponding cutting guides. The fibular segments were transferred and fixed to the pre-bent plate, seating the reconstructed arch within the pre-established spatial framework and obviating the need for intraoperative navigation.

2.5 Accuracy Evaluation

Postoperative CBCT imaging was performed at approximately ten days following surgery. The resulting datasets were used to generate three-dimensional surface models, which were subsequently registered against the preoperative VSP in Materialise 3-matic software. Superimposition was anchored on unoperated native mandibular regions to ensure accurate spatial alignment.

Spatial deviations between the postoperative anatomy and the virtual plan were quantified at predefined anatomical landmarks, with linear discrepancies measured in millimeters. Rather than relying on a single aggregate distance metric, deviations were decomposed into directional components along three orthogonal axes: the X-axis (mediolateral), Y-axis (superoinferior), and Z-axis (anteroposterior). Surface-based deviation mapping was performed using color-coded heatmaps, enabling visual identification of zones with the greatest geometric discordance.

2.6 Statistical Analysis

All math and data tracking went through SPSS version 26.0. We kept things simple and reported continuous numbers as a mean plus or minus the standard deviation. We also needed to know if bigger surgical defects led to worse accuracy. We split the patient list using the Brown classification. People with Class I or II defects went into a "Less Complex" bracket. Those with Class III or IV defects formed the "Complex" bracket. To see if the size of the defect actually worsened the reconstruction, we compared the average deviation numbers of the two patient cohorts. We handled this comparison using a standard independent t-test. Any resulting probability value (P-value) under 0.05 meant the difference was mathematically real, not just a random coincidence.

Result and discussions

3.1 Patient Characteristics The study cohort comprised 12 consecutive patients (6 male, 6 female) with a mean age of 45.8 years (range 17–78; SD ± 14.8). The primary surgical indication was extensive benign pathology in nine cases, including ameloblastoma, ossifying fibroma, and fibrous dysplasia. The remaining three patients underwent resection for squamous cell carcinoma. All 12 patients underwent successful fibula free flap reconstruction without total flap loss during the observation period. Full demographic and surgical parameters are presented in Table 1.

By Brown classification, six patients presented with less complex defects (Class I–II) and six with complex defects (Class III–IV), yielding an equal distribution across defect severity categories.

Table 1*Brown classification: Class I-II (Less Complex), Class III-IV (Complex). (SCC: Squamous Cell Carcinoma; R: Recurrent).

Pt No.	Sex/ Age	Diagnosis	Brown Class*	Fibula Segments	Mean Deviation (mm)	Max Deviation (mm)	Region of Max Error
1	F/59	Ameloblastoma	III	3	2.30	4.40	Condyle
2	F/29	Ossifying Fibroma	I	2	3.04	4.24	Angle
3	F/17	Fibrous Dysplasia	IV	2	3.38	6.13	Condyle
4	F/43	Osteonecrosis	IV	4	3.50	9.99	Condyle
5	F/32	Ameloblastoma	Ic	2	4.88	12.10	Ramus / Neocondyle
6	M/38	Ameloblastoma (R)	II	2	4.80	9.68	Ramus / Angle
7	M/54	SCC (T3N0M0)	III	3	5.14	10.36	Ramus / Condyle
8	F/40	Fibro-oss. Lesion	III	3	2.22	3.32	Ramus
9	F/78	SCC (Floor of Mouth)	III	3	3.19	6.14	Symphysis
10	M/55	Ameloblastoma	I	3	3.68	6.10	Lower Border / Body
11	M/56	Ameloblastoma (R)	Ic	2	2.34	11.44	Symphysis (Loose Bone)
12	M/56	Ameloblastoma (R)	Ic	2	2.35	3.49	Condyle
MEAN	45.8y	-	-	-	3.40 ± 1.02	7.28 ± 3.15	Posterior Proximal (83%)

3.2 Accuracy of Reconstruction and Global Error

The mean global 3D deviation across the entire cohort was 3.40 mm (SD = 1.02). To assess the effect of defect complexity on overall accuracy, patients were stratified by Brown classification. The less complex subgroup (Class I–II) recorded a mean deviation of 3.55 mm (± 1.12), while the complex subgroup (Class III–IV) recorded 3.29 mm (± 1.10). Independent samples t-test yielded a P-value above 0.05, indicating no statistically significant difference in global accuracy between the two subgroups. However, this aggregate metric does not reflect the anatomically localized geometric failures identified by region-specific analysis.

3.3 Regional Error Distribution

Surface-based heatmap analysis demonstrated a consistent spatial pattern of deviation across the cohort. Anterior segments (symphysis and mandibular body) showed relatively low deviation, with most values below 3 mm. In contrast, maximum deviations were concentrated in the posterior zones in ten of twelve cases, with errors localized predominantly to the *ramus* and *the condylar head*. The maximum recorded condylar deviation in this cohort was 12.10 mm (Patient 5), illustrating the degree of spatial instability that can occur in a proximally unsupported segment following condylectomy [11].

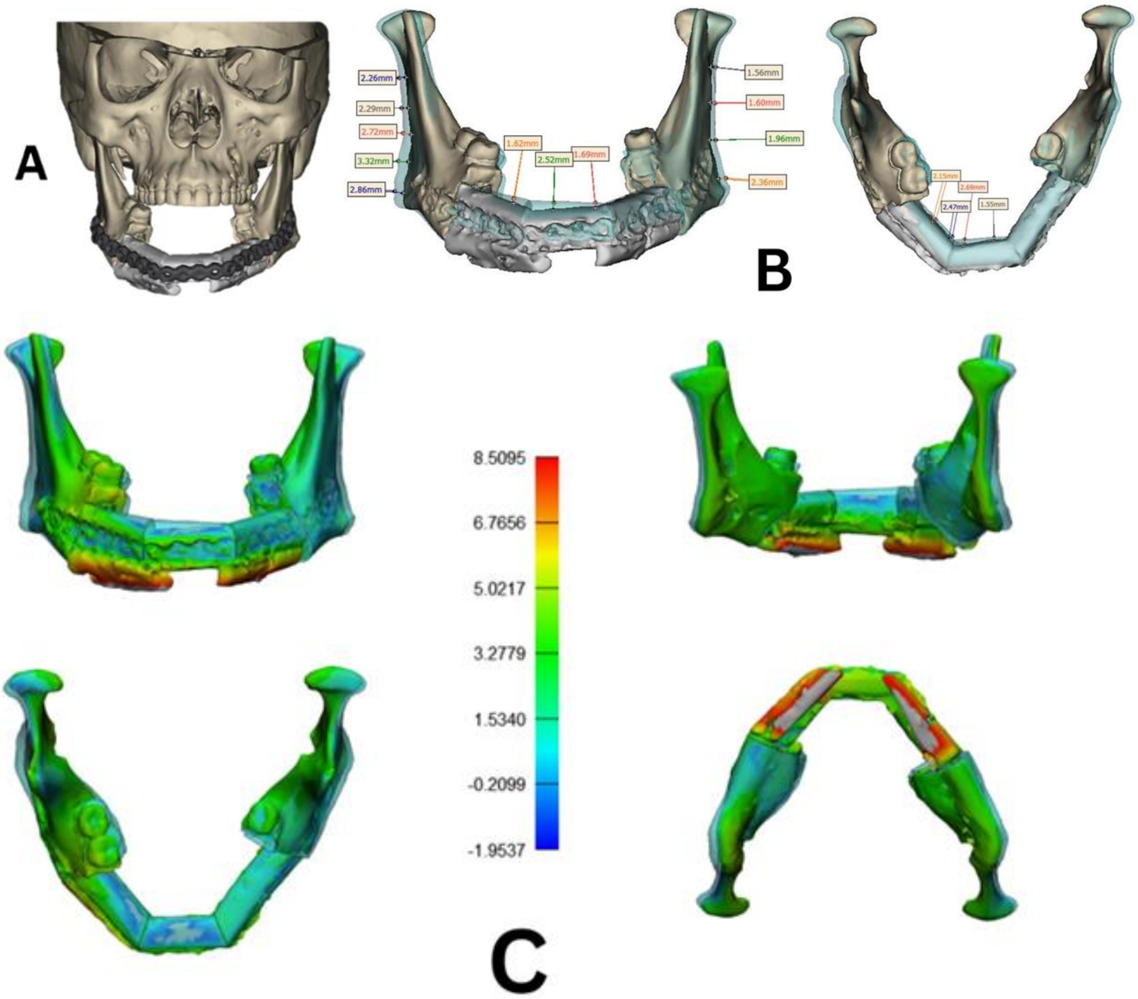

Figure 1. Quantitative 3D accuracy evaluation of VSP-guided mandibular reconstruction. (A) Postoperative 3D skeletal rendering illustrating the reconstructed mandible utilizing fibular segments rigidly fixed with a pre-bent titanium reconstruction plate. (B) Surface-based superimposition of the postoperative 3D model (solid/plate) onto the preoperative virtual surgical plan (translucent). The callout boxes display specific point-to-point linear deviations (in millimeters) along the bilateral contours. (C) 3D color-coded heatmap analysis quantifying the global surface deviations. The predominantly green and light blue zones indicate high spatial concordance across the reconstructed arch, while warmer colors highlight localized areas of geometric discrepancy.

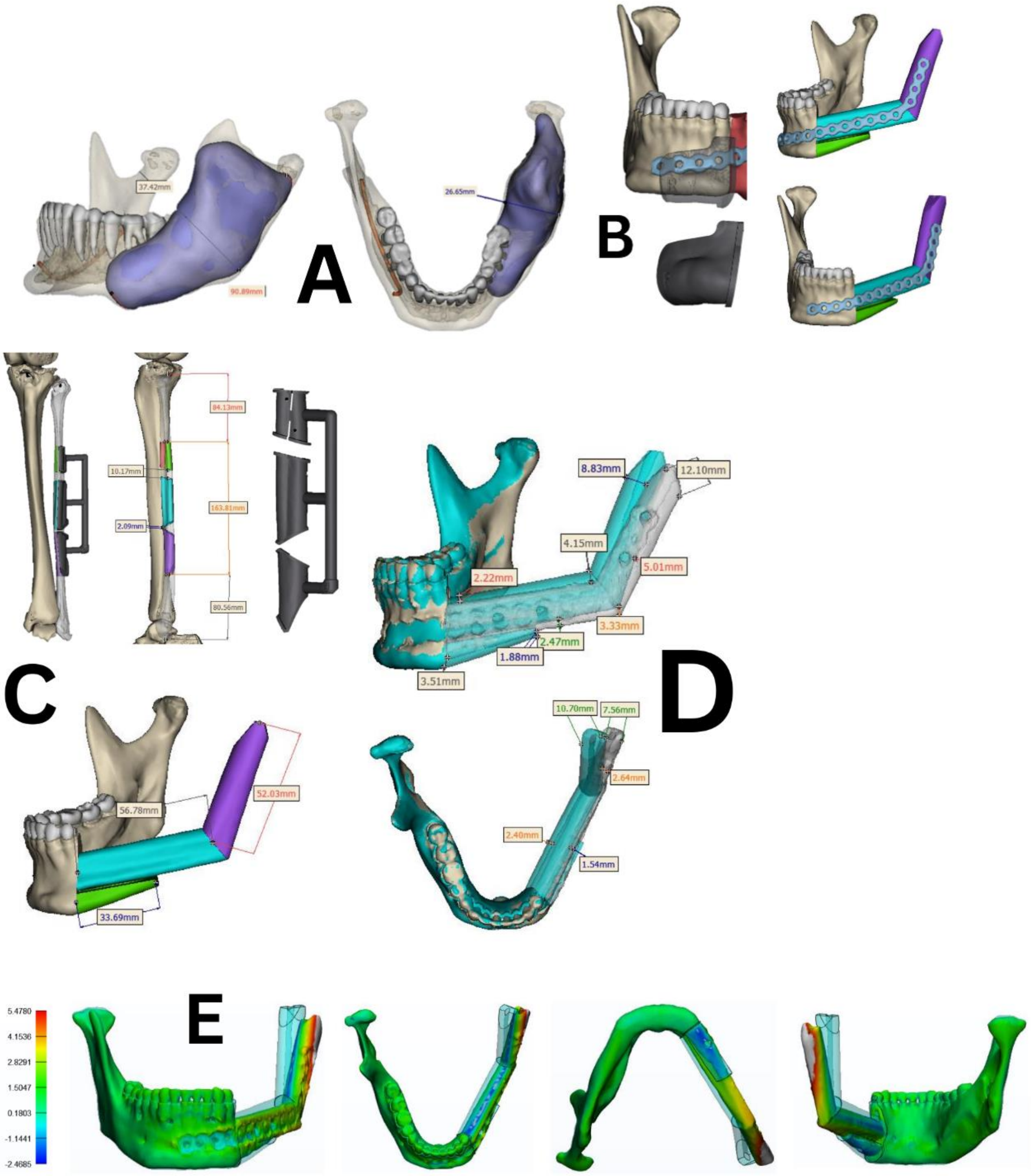

Figure 2. Directional error analysis in a complex reconstruction involving condylar resection (Patient 5). (A) Preoperative 3D reconstruction showing the extensive tumor (blue) involving the left ramus and condyle. (B, C) Virtual Surgical Plan (VSP) detailing the cutting guides and two-segment fibular neocondyle design. (D) Superimposition of the postoperative CT (cyan) onto the VSP (translucent). Linear measurements show severe lateral displacement of the proximal segment (up to 12.10 mm). (E) 3D heatmap confirming massive lateral flaring (red zones), illustrating the biomechanical instability of a non-rigidly fixed neocondyle within the glenoid fossa.

3.4 Directional Error Trends and Biomechanical Implications

Axis-specific decomposition of the 3D deviations provided mechanistic insight into the regional failure patterns summarized in Table 2.

Transverse Plane (X-axis): Posterior proximal segment displacement along the mediolateral axis manifested in two mechanically opposing patterns. Five patients (Patients 3, 7, 8, 10, and 11) exhibited *medial displacement*, classified as medial collapse. In the absence of rigid proximal stabilization, the contractile vector of the medial pterygoid muscle displaced the proximal segment *inward*. In four patients (Patients 4, 5, 6, and 12), the proximal segments displaced *outward* in a *lateral flare*. The maximum lateral deviation of 9.13 mm was recorded in Patient 5, in whom the fibular neocondyle *was laterally displaced* from its planned position within the glenoid fossa.

Table 2. Directional Error Analysis and Regional Displacement Patterns (Transposed).

Pt No.	Posterior/ Proximal Zone (Condyle/ Ramus/ Angle)	ΔX Medio-lateral)	ΔY (Supero-inferior)	ΔZ (Antero-posterior)	Anterior / Distal Zone (Body / Symphysis)	ΔX (Medio-lateral)	ΔY (Supero-inferior)	ΔZ (Antero-posterior)	Pre-dominant Deformity Pattern
1	Condyle/ Ramus	+1.96	+2.81	±1.56	Body/ Symphysis	—	-2.57	—	Yaw/ Sagging
2	Angle/Body	−2.37	+3.30	+2.87	Symphysis	+0.17	—	+3.96	Medial Collapse
3	Condyle/ Ramus	−4.76	+5.17	−3.04	Symphysis	—	-3.09	-2.03	Postero-medial
4	Condyle	+9.99	−2.91	−2.60	Symphysis	+7.45	−3.49	+3.03	Lateral Flaring
5	Neocondyle	+9.13	—	−10.49	Angle/ Body	+2.64	−3.74	-5.01	Fossa Mismatch
6	Condyle/ Angle	+4.04	−4.02	±6.60	Symphysis	+2.54	−6.98	+3.93	Rotational Twist
7	Condyle/ Ramus	−8.21	—	−8.93	Symphysis	−1.33	+5.03	—	Postero-medial
8	Angle/ Ramus	−2.85	—	—	Symphysis	—	−1.94	+2.28	Medial Shift
9	Angle/ Body	±2.41	+4.41	±2.18	Symphysis	−3.13 / +4.54	+5.65	+5.13	Over-closure
10	Angle	−2.62	−2.97	−2.37	Body/ Symphysis	−5.67	−3.49	—	Medial Collapse
11	Condyle/ Ramus	−3.31	+2.68	−3.13	Symphysis	+4.70	−2.71	−10.38*	Twisting/ Loose
12	Condyle/ Ramus	+2.37	−3.49	−2.37	Body/ Symphysis	−1.64	−2.90	—	Drift & Collapse
Mean ± SD (signed)	—	+0.48 ± 5.51	+0.55 ± 3.79	−1.79 ± 5.00	—	+1.49 ± 4.00	−1.84 ± 3.78	+0.11 ± 5.46	—
|Mean| ± SD	—	4.50 ± 2.91	3.53 ± 0.84	4.19 ± 3.04	—	3.41 ± 2.34	3.78 ± 1.51	4.47 ± 2.65	—
Max |deviation|	—	+9.99	+5.17	−10.49	—	+7.45	−6.98	−10.38	—

*Table 1*Note: The extreme posterior deviation (-10.38 mm) at the symphysis in Patient 11 correlates with a mobile, non-rigidly fixed bone fragment retracted by the suprahyoid musculature.*

Vertical Plane (Y-axis): Inferior displacement of the symphyseal and body segments was identified in seven of twelve patients, a pattern designated as inferior sagging. The maximum inferior deviation of 6.98 mm was recorded in Patient 6, reflecting the combined gravitational and soft tissue load exerted by the vascularized paddle. Conversely, Patients 7 and 9 demonstrated superior displacement, consistent with an over-closed position. In Patient 9, the surgical resection of the oral floor involved the mandibular depressor muscles, resulting in an unopposed superiorly directed force from the elevator muscles.

Sagittal Plane (Z-axis): Posterior displacement along the anteroposterior axis was predominantly observed in the proximal segments. Seven patients demonstrated posterior drift of the ramus. The most pronounced Z-axis deviation was recorded in Patient 11, where an acute posterior displacement of 10.38 mm at the anterior symphysis was attributed to hardware destabilization and unopposed suprahyoid muscle contraction.

Discussion

4.1 General Accuracy and Comparability

The mean global deviation of 3.40 ± 1.02 mm observed in this cohort is consistent with values reported in comparable studies of VSP-guided fibula free flap reconstruction. Bengur et al. reported a mean deviation of 2.8 mm using CAD/CAM workflows, while Annino et al. documented accuracy values in the range of 2.5–4.2 mm across similar defect categories. [7,15] The present results therefore confirm that the VSP protocol utilized here achieves a level of global accuracy that is both clinically acceptable and reproducible. However, global deviation metrics alone provide an incomplete characterization of surgical fidelity. Region-specific analysis demonstrated that aggregate accuracy measures may obscure clinically significant localized displacements that carry direct implications for condylar positioning, occlusal rehabilitation, and facial symmetry.

No statistically significant difference in mean deviation was identified between the less complex (Brown Class I–II: 3.55 ± 1.12 mm) and complex (Brown Class III–IV: 3.29 ± 1.10 mm) subgroups ($P > 0.05$). This finding is consistent with Padilla et al., who similarly demonstrated that defect complexity does not significantly affect overall reconstruction accuracy when a standardized CAD/CAM workflow is employed. [8] The reproducibility across defect categories is attributed to the pre-operative plate adaptation protocol, which effectively removes the most technically demanding contouring steps from the intraoperative environment. Despite this favorable global consistency, the present axis-specific analysis reveals that the pattern and direction of residual error vary considerably by anatomical zone—a distinction that aggregate metrics fail to capture.

4.2 Proximal Segment Instability: Medial Collapse vs. Lateral Flaring

Proximal segment instability emerged as the predominant source of geometric discordance in this series, with 83% of maximum deviations localized to the condylar and ramal regions. This finding is consistent with the observations of Anderson et al. and Becktor et al., who identified the proximal segment as the most mechanically vulnerable component of mandibular reconstruction due to loss of anterior bony continuity and the resultant exposure of the segment to unopposed muscular forces. [11,18] Segmental resection converts the condyle into an isolated anatomical unit, and the subsequent absence of skeletal continuity renders it susceptible to displacement along the transverse axis. In the present cohort, this instability manifested in two mechanically distinct and directionally opposed patterns.

Medial collapse, observed in five cases (Patients 3, 7, 8, 10, and 11), was the more frequently encountered transverse displacement pattern. The medial pterygoid muscle is the primary biomechanical driver of this displacement; in the absence of rigid proximal stabilization, its contractile vector displaces the ramus medially and posteriorly. This mechanism aligns with the transverse displacement patterns described by Becktor et al. following sagittal split osteotomies, in which proximal segment control was similarly compromised when fixation was insufficient. [18]

Lateral flaring was identified in four cases (Patients 4, 5, 6, and 12) and represented the inverse displacement pattern. Patient 5, who underwent total condylectomy with fibular neocondyle reconstruction, demonstrated the most pronounced lateral deviation of 9.13 mm, with the reconstructed articular head failing to maintain its intended position within the glenoid fossa. The biomechanical basis for this pattern involves the unopposed lateral and superior traction of the temporalis and lateral pterygoid muscles in the absence of a stable articular seat. This is corroborated by the condylar repositioning literature; Chow et al. demonstrated that without active intraoperative condylar seating maneuvers, geometric fidelity of the reconstructed articular unit cannot be reliably maintained. [19] The geometric mismatch between a linear fibular strut and the concave morphology of the cranial base further compounds this instability. These findings collectively support the selective use of temporary maxillomandibular fixation or customized joint-positioning stents as adjunctive intraoperative measures for cases involving condylar resection.

4.3 Anterior Arch Vulnerability: Inferior Displacement and Atypical Vertical Deviations

Vertical displacement analysis along the Y-axis identified inferior migration of the anterior arch as a consistent finding, observed in seven of twelve cases. The symphyseal and mandibular body segments demonstrated inferior displacement from their planned positions, with the maximum deviation of 6.98 mm recorded in Patient 6. This pattern is primarily attributable to the combined gravitational loading imposed by the vascularized fascio-cutaneous paddle and the persistent inferior traction exerted by the suprahyoid musculature—specifically the digastric and geniohyoid complexes. Gil-Marques et al. have described analogous inferior displacement vectors in bone graft constructs subject to soft tissue tension, noting that the magnitude of displacement correlates with the volume of the associated soft tissue component. [9] The anterior arch, being mechanically unsupported in the midline and exposed to bilateral cervical muscular traction, is therefore inherently predisposed to inferior migration in the early postoperative period.

Atypical vertical displacements were recorded in two cases and illustrate the mechanical consequences of altered muscular anatomy following oncological resection. Patient 9 demonstrated a superior over-closure of +5.65 mm, a displacement directly attributable to the resection of the floor of mouth and the consequent loss of the suprahyoid depressor complex. The elimination of inferior counter-traction resulted in unopposed superior displacement by the elevator musculature. This mechanism has been described in the context of mandibular reconstruction following floor-of-mouth oncological procedures, where extensive soft tissue resection fundamentally alters the postoperative muscular force balance. [11] Patient 11 demonstrated a posterior symphyseal displacement of 10.38 mm following hardware destabilization at the osteotomy interface. In the absence of adequate plate fixation, the unopposed contraction of the geniohyoid and digastric musculature generated the most pronounced single-point deviation in this series. This case illustrates the critical importance of multi-point anterior fixation, as standard reconstruction plates may be insufficient to resist the combined cervical and masticatory loading concentrated at the symphysis, particularly in cases where bone contact at the osteotomy is suboptimal.

4.4 VSP in Secondary and Salvage Reconstruction

The deliberate inclusion of secondary and salvage reconstructions in this study—including cases complicated by osteonecrosis, recurrent malignancy, and complete absence of native anatomical landmarks—provides clinically relevant data on VSP performance under maximally distorted operative conditions. In these cases, the preoperative digital workflow served a fundamentally different function than in primary reconstruction. Rather than augmenting or refining a conventional surgical plan, the CAD/CAM model constituted the primary spatial reference framework, as no reliable native skeletal architecture remained for intraoperative orientation. Shalabi et al. similarly highlighted the indispensability of VSP in revision cases, noting that the technology’s value increases proportionally with the degree of anatomical distortion. [5] Notably, the mean deviations recorded in the salvage cases within this cohort (Brown Class III–IV) were statistically comparable to those in primary reconstructions ($P > 0.05$), confirming that the VSP-guided protocol maintains its accuracy under these challenging conditions. This finding has direct clinical implications for institutions managing high proportions of recurrent or osteonecrotic mandibular pathology, for whom a reliable, reproducible workflow is most critically needed.

4.5 Cost-Effectiveness of Pre-bent Plates

Patient-specific milled titanium implants currently represent the highest technical standard for reconstructive precision. [13] However, their substantial manufacturing costs and extended lead times restrict their routine clinical application, particularly in resource-limited settings and high-volume oncological centers. [14] The present study validates a pragmatic intermediate approach: the manual pre-operative adaptation of standard titanium reconstruction plates against patient-specific stereolithographic resin models. This technique relocates the technically demanding plate-contouring procedure to the pre-operative phase, thereby reducing intraoperative time and minimizing the technical variability introduced by fatigue-dependent freehand bending. The mean deviation of 3.40 mm achieved with this methodology is comparable to values reported by Bengur et al. using full CAD/CAM fabrication, suggesting that pre-bent conventional hardware represents a viable and economically accessible alternative. [7] For institutions where patient-specific implants are not routinely available, this protocol provides a reproducible framework that does not require significant additional infrastructure investment beyond existing CT imaging and model-printing capabilities.

4.6 Limitations

The interpretation of these findings is subject to several methodological limitations. The retrospective design and the limited cohort size of 12 patients restrict the statistical power of the directional error analysis and preclude broad generalization of the observed biomechanical trends to larger populations. While the sample size is consistent with comparable single-institution feasibility studies in this subspecialty, prospective multi-centre data will be necessary to confirm the regional displacement patterns identified here. Additionally, the severity of pre-existing pathology—particularly in cases of advanced osteonecrosis or recurrent malignancy—may have introduced systematic confounding by distorting the soft tissue envelope and underlying bony architecture at the time of pre-operative CT acquisition. This distortion would propagate into the virtual surgical plan as a baseline geometric inaccuracy that cannot be fully corrected by the planning workflow. Future investigations should incorporate intraoperative navigation systems to enable real-time spatial feedback during segment positioning, which may be particularly valuable for stabilizing the proximal segment and monitoring anterior arch position prior to final fixation. Finite element modelling of the identified muscular force vectors may also yield quantitative data to guide the development of more mechanically optimized fixation hardware.

Conclusion

The combined application of virtual surgical planning, patient-specific SLA cutting guides, and pre-operatively adapted titanium reconstruction plates constitutes a reproducible and accurate framework for VSP-guided mandibular reconstruction with fibula free flaps. The mean global 3D deviation of 3.40 ± 1.02 mm recorded across this cohort is consistent with published benchmarks and was maintained irrespective of defect complexity, confirming that a standardized digital workflow preserves reconstructive fidelity even in extensive Brown Class III–IV defects and complex salvage cases. The primary contribution of this study, however, lies in demonstrating that global accuracy metrics are insufficient to characterize the true biomechanical performance of the reconstruction. Axis-specific analysis revealed that the signed mean deviations along the X- and Y-axes approach zero—a statistical artifact produced by opposing directional errors that cancel one another out—whereas the corresponding absolute mean deviations reached 4.50 ± 2.91 mm (posterior ΔX) and 3.78 ± 1.51 mm (anterior ΔY). This divergence confirms that aggregated global accuracy scores systematically obscure clinically significant, zone-specific geometric failures.

The directional analysis identified two mechanically distinct and anatomically localized failure patterns. In the posterior region, segmental resection converts the condyle and ramus into an unsupported anatomical unit, rendering it susceptible to unopposed masticatory muscle traction. This produced medial collapse in five patients, driven by the contractile vector of the medial pterygoid, and lateral flaring in four others following condylectomy, where the absence of a stable articular seat permitted temporalis and lateral pterygoid forces to displace the neocondyle laterally by up to 9.13 mm. In the anterior region, inferior displacement of the symphyseal and body segments was identified in seven of twelve cases, with a maximum vertical drop of 6.98 mm attributable to gravitational loading compounded by the mass of the vascularized fascio-cutaneous paddle and the inferior traction of the suprahyoid musculature. Taken together, these findings establish that the biomechanical vulnerability of a reconstruction is determined by anatomical location and the local muscular force environment, not by overall defect size.

These findings have direct implications for surgical planning and hardware selection. Standard (SLA) Stereolithography cutting guides accurately execute the planned osteotomies but provide no mechanism for resisting the postoperative muscular forces that subsequently displace the free segments. For cases involving condylar resection, adjunctive intraoperative condylar seating maneuvers—such as temporary maxillomandibular fixation or customized articular positioning stents—should be incorporated into the surgical protocol prior to final plate fixation. For complex anterior reconstructions, multi-point fixation strategies that address the inferior muscular traction vectors warrant prospective evaluation. Future studies employing intraoperative navigation and finite element modelling of patient-specific muscular force distributions will be necessary to translate these biomechanical observations into evidence-based fixation protocols.

LIST OF REFERENCES:

1. Fatani B, Fatani J, Fatani OA. Approach for mandibular reconstruction using vascularized free fibula flap: a review of the literature. *Cureus*. 2022 Oct;14(10):e30161. doi:10.7759/cureus.30161
2. Wei W. The utility of vascularized free fibula flap in mandibular reconstruction. В оригинале DOI не нашёлся для этой конкретной работы с автором Wei W; однако широко цитируемая статья Peled et al. об использовании фибулы имеет DOI: 10.1016/j.joms.2004.06.052 (что относится к другому исследованию по аналогичной теме).
3. Shroff S, Nair S, Shah A, Kumar B. Versatility of fibula free flap in reconstruction of facial defects: a center study. J Maxillofac Oral Surg. 2017 Jan;16(1):101–107. doi:10.1007/s12663-016-0930-6
4. Duchscherer J, Aalto D, Westover L. Evaluation of facial symmetry after jaw reconstruction surgery. Comput Methods Biomech Biomed Engin. 2021 Jan;24(2):193–201. doi:10.1080/10255842.2020.1870965
5. Shalabi MM, Darwich K, Kheshfeh MN, Hajeer MY. Efficiency and applicability of virtual surgical planning in maxillofacial and mandibular bone reconstruction: a narrative review. Clin Pract. 2025 Mar;15(3):62. doi:10.3390/clinpract15030062
6. Li B, Wei H, Jiang T, Qian Y, Zhang T, Yu H, et al. Randomized clinical trial of the accuracy of patient-specific implants versus CAD/CAM splints in orthognathic surgery. *Plast Reconstr Surg*. 2021 Nov;148(5):1005–1016. doi:10.1097/PRS.0000000000008427
7. Bengur FB, Humar P, Saadoun R, Khan N, Anstadt EE, Dang S, et al. Computer-aided design and manufacturing in free fibula reconstruction of the mandible: comparison of long-term outcomes. Plast Reconstr Surg. 2024 Oct;154(4):801–812. doi:10.1097/PRS.0000000000011701
8. Padilla PL, Mericli A, Largo R, Garvey P. Computer-aided design and manufacturing versus conventional surgical planning for head and neck reconstruction: a systematic review and meta-analysis. Plast Reconstr Surg. 2021 Jun;147(6):1143–1155. doi:10.1097/PRS.0000000000008085
9. Gil-Marques B, Pallarés-Sabater A, Brizuela-Velasco A, Lasheras FS, Lázaro-Calvo P, Gómez-Adrián MD, et al. A biomechanical analysis of the influence of the morphology of the bone block grafts on the transfer of tension or load to the soft tissue by means of the finite elements method. Materials (Basel). 2022 Dec;15(24):9039. doi:10.3390/ma15249039
10. Hinrichsen N, Birk-Sørensen L, Gottrup F, Hjortdal V. Wound contraction in an experimental porcine model. Scand J Plast Reconstr Surg Hand Surg. 1998 Sep;32(3):245–250. doi:10.1080/02844319850158561
11. Anderson SR, Pak KY, Vincent A, Ong AA, Ducic Y. Reconstruction of the mandibular condyle. Facial Plast Surg. 2021 Apr;37(2):220–227. doi:10.1055/s-0041-1726444
12. Kodama M, Ozawa M, Mitsuhashi T, Kawasaki Y. Condyle dislocation following mandibular reconstruction using a fibula free flap: complication cases. Maxillofac Plast Reconstr Surg. 2019;41:14. doi:10.1186/s40902-019-0197-1
13. Dérand P, Rönnér LE, Hirsch J. Imaging, virtual planning, design, and production of patient-specific implants and clinical validation in craniomaxillofacial surgery. Facial Plast Surg. 2012 Sep;28(5):543–551. doi:10.1055/s-0032-1313357
14. Mishra AK. From injection molding to 3D printing of patient-specific implants. Biomed J Sci Tech Res. 2018 Aug;8(3):1660. doi:10.26717/BJSTR.2018.08.001660
15. Annino D, Sethi RKV, Hansen EE, Horne S, Dey T, Rettig EM, et al. Virtual planning and 3D-printed guides for mandibular reconstruction: factors impacting accuracy. Laryngoscope Investig Otolaryngol. 2022 Oct;7(5):1410–1418. doi:10.1002/lio2.830
16. Zavattero GP, Gerbino M, Ramieri C, Berrone G. Step-by-step mandibular reconstruction with free fibula flap modelling. J Craniomaxillofac Surg. 2013 Jan;41(1):e1–e8.
17. Ferri ER, Lelkes B, Yates E. Optimizing functional outcomes in mandibular condyle reconstruction with the free fibula flap using computer-aided design and manufacturing technology. J Oral Maxillofac Surg. 2018 Mar;76(3):611–619.
18. Becktor J, Rebellato J, Becktor K, Isaksson S, Vickers PD, Keller E. Transverse displacement of the proximal segment after bilateral sagittal osteotomy. J Oral Maxillofac Surg. 2002 Apr;60(4):395–401. doi:10.1053/joms.2002.31227
19. Chow W, He Z, Liu Y, Song J, Xu C, Luo E. Intraoperative condylar positioning techniques on mandible in orthognathic surgery. Orthod Craniofac Res. 2022 Feb;25(1):83–92. doi:10.1111/ocr.12568

Entered 20.01.2026